JAERI-M
86-036

PARTICLE CONTROL IN A TOKAMAK

March 1986

Seio SENGOKU

日本原子力研究所
Japan Atomic Energy Research Institute

JAERI-Mレポートは，日本原子力研究所が不定期に公刊している研究報告書です。
入手の問合わせは，日本原子力研究所技術情報部情報資料課（〒319－11茨城県那珂郡東海村）あて，お申しこしください。なお，このほかに財団法人原子力弘済会資料センター（〒319-11茨城県那珂郡東海村日本原子力研究所内）で複写による実費頒布をおこなっております。

JAERI-M reports are issued irregularly.
Inquiries about availability of the reports should be addressed to Information Division, Department of Technical Information, Japan Atomic Energy Research Institute, Tokai-mura, Naka-gun, Ibaraki-ken 319-11, Japan.

編集兼発行　日本原子力研究所
印　　刷　日立高速印刷株式会社

JAERI-M 86-036

PARTICLE CONTROL IN A TOKAMAK

Seio SENGOKU
Department of Thermonuclear Fusion Research,
Naka Fusion Research Establishment
Japan Atomic Energy Research Institute
Naka-machi, Naka-gun, Ibaraki-ken

(Received January 31, 1986)

A survey of the studies on particle control, for both impurity and fuel particles, on DIVA and Doublet III tokamaks is presented. Relation between plasma-wall interactions and confinement characteristics of a tokamak plasma with respect to both impurity and fuel particle controls is discussed. It is shown as examples of particle control that energy confinement time is improved by impurity control with carbonization in DIVA and by fuel particle control with D_2 pellet injection in Double III.

Keywords: Particle Control, Impurity, Fuel, Energy Confinement, Carbonization, DIVA, Pellet Injection, Doublet III, Tokamak Plasma

トカマクにおける粒子制御

日本原子力研究所那珂研究所核融合研究部
仙石　盛夫

（1986年1月31日受理）

ＤＩＶＡ及びDoublet Ⅲトカマクにおける不純物及び燃料粒子制御に関する研究をまとめた。プラズマ・壁相互作用と閉込め特性の関連性について，不純物及び粒子制御の観点から議論した。粒子制御の例として，ＤＩＶＡにおける炭素壁による不純物制御により，又Doublet Ⅲにおける重水素ペレット入射による燃料粒子制御により共にエネルギー閉込め時間が改善されることを示した。

那珂研究所：茨城県那珂郡那珂町大字向山

Contents

目　　次

A survey of the studies on particle control, for both impurity and fuel particles, on DIVA and Doublet III tokamaks is presented.

Relation between plasma-wall interactions and confinement characteristics of a tokamak plasma with respect to both impurity and fuel particle controls is discussed.

Following results are obtained from impurity control studies:

(1) Physical models of boundary/divertor plasma and of divertor functions about impurity control are empilically obtained. By a computer simulation based on above model with respect to divertor functions for JT-60 tokamak, it is found that the allowable electron temperature of the divertor plasma is not restricted by a condition that the impurity release due to ion sputtering does not increase continuously. In this case, it is necessary to consider how to cope with handling heat load and erosion of a divertor plate.

(2) Dense and cold divertor plasma accompanied with strong remote radiative cooling was diagnosed along the magnetic field line in the simple poloidal divertor of Doublet III tokamak. Strong particle recycling region is found to be localized near the divertor plate. In such a system, the heat load and the erosion by ion sputtering of the divertor plate are decreased.

(3) By applying carbon coating on entire first wall of DIVA tokamak, dominant radiative region is concentrated more in boundary plasma resulting a hot peripheral plasma with cold boundary plasma. Energy confinement time of such a plasma is improved by a factor of two due to increasing of the effective radius of the core plasma by applying a carbon wall;

and from particle control studies:

(1) The INTOR scaling on energy confinement time is applicable to high density region when a core plasma is fueled directly by solid deuterium pellet injection in Doublet III tokamak.

(2) As remarkably demonstrated by direct fueling with pellet injection, energy confinement characteristics can be improved at high density range by decreasing particle deposition at peripheral plasma in order to reduce plasma-wall interaction.

(3) If the particle deposition at boundary layer is necessarily reduced, the electron temperature at the boundary or divertor region increases due to decrease of the particle recycling and the electron density there. At that situation, the enhancement of impurity release can be the serious problem and thus some kind of "localized" control of particle or impurity at the boundary or near the divertor plate should be applied.

The controls of not only impurities but also fuel particles are important as shown above. Improvement of energy confinement time is demonstrated to be possible by controlling both impurity and fuel particles.

Required atomic data base for studying above scheme is presented at the last section.

1. BOUNDARY AND DIVERTOR PLASMAS

1.1 Characteristics [1,2,3,4,5]

In order to recognize the "impurity control", the following closed, cyclic processes are important (Fig.1): (1)the role of the boundary plasma on the production of impurities; (2)impurity transport in the boundary plasma and impurity flow into the main plasma; and (3)influences of accumulated impurities on the main and the boundary plasma. All of these processes and impurity control are deeply connected to the "boundary plasmas". Therefore, it is very important to understand the boundary plasma. The possible controls on those processes are also shown in the figure with important parameters in boundary plasma: temperature and density of the boundary plasma (T_b and n_b), particle flow velocity, v_f, and electric field, $E_{//}$, parallel to the magnetic field lines and the parpendicular particle diffusion coefficient , $D_\perp$.

The plasma interacts with the surrounding first walls, including limiter/divertor-neutralizer-plates, in various ways, e.g. sputtering by ions and charge-exchange neutrals and arcing. These processes strongly depend on the boundary plasma, i.e. limiter or divertor scrape-off plasmas. In this section we summarize the characteristics of the boundary plasmas.

Boundary plasma parameters are related to the main plasma through energy and particle balance. The energy balance in the stationary phase of a tokamak discharge is as follows. Total input power, P_{IN}, is balanced with these loss processes such as radiation and charge-exchange, P_R and P_{CX}, to the entire wall, and conduction-convection loss, P_{CC}, mainly onto the limiter/divertor neutralizer plate. Therefore, it can be expressed as,

$$P_S = P_{IN} - P_R - P_{CX} = P_{CC} \tag{1}$$

Here the power loss onto the surface, P_S, is the integral of local heat flux, q, as $P_S = \int q ds$. Then, the problem is how to evaluate q.

From a normal sheath theory the heat flux is given by the following equation[6]:

$$q = \gamma f_p T_e , \tag{2}$$

where f_p is the particle flux density onto the material surface and γ is the heat transmission rate across the sheath including the effects of the sheath potential, αT_e, secondary electron emission coeffcient, δ, and the correction to the distribution function, F and F'. That is:

$$\gamma = \left\{ 2 \left(\frac{1}{1-\delta} + 1 \right) + \alpha \right\} F , \tag{3}$$

$$\alpha = -\ln \frac{\xi \sqrt{m/M}}{1-\delta} \cdot F' , \tag{4}$$

where ξ is the ratio of the electron to ion saturation currents, and m and M are the electron and ion masses, respectively. The value F exceeds 10 in a runaway discharge, but is around unity in a normal discharge. F' is also around unity in a normal discharge. The maximum value of δ is given by space charge limit[6] as $\delta_{max} = 1 - 8.3\sqrt{m/M}$ and is 0.81 for hydrogen and 0.86 for deuterium plasmas. Corresponding to this, γ varies between 6.7-13.5(H) and 7.0-17.0(D), respectively, in a normal discharge.

As long as the sheath is formed on the material surface, the total power loss onto the material surface is then deduced as:

$$P_S = \int q ds = F_p \gamma \bar{T}_b \tag{5}$$

where $F_p \equiv N_p/\bar{\tau}_p$ is the total particle outflux, $\bar{\tau}_p$ the overall particle confinement time, and $\bar{T}_b$ the average boundary temperature. Then, the power balance, eq.(1), can be rewritten as

$$\gamma \frac{N_p}{\bar{\tau}_p} \bar{T}_b = P_{IN} - P_R - P_{CX}$$

$$= \frac{3}{2} \frac{N_p}{\bar{\tau}_E} (\bar{T}_i + \bar{T}_e) - P_R - P_{CX},$$

where $\bar{T}_i$ and $\bar{T}_e$ are the average ion and electron temperatures in the main plasma. From this, we can obtain the relation between the boundary temperature and the core temperature as

$$\bar{T}_b = \frac{3}{\gamma} \frac{\bar{\tau}_p}{\tau_E} \left(1 - \frac{P_R + P_{CX}}{P_{IN}}\right) \bar{T} \quad (\bar{T} = \bar{T}_i + \bar{T}_e) \tag{6}$$

Other important parameters are the width of the scrape-off layer, d, average boundary density, $\bar{n}_b$, and particle flux density, f_p, as

$$d = \sqrt{D_\perp L / v_f}\ , \tag{7}$$

$$\bar{n}_b = \frac{1}{2} \frac{L}{v_f} \frac{a}{d} \frac{\bar{n}_e}{\bar{\tau}_p}\ , \tag{8}$$

$$f_p = v_f\ \bar{n}_b\ , \tag{9}$$

and the electric field, E. a is the plasma radius, $D_\perp$ the perpendicular diffusion coefficient and L and v_f are the path length of the charged particles and parallel flow velocity along the field line in the scrape-off layer. Among these parameters, the essential parameters are γ, v_f, $D_\perp$, and E. These are reasonably obtained in DIVA tokamak: $\gamma \simeq 7$, $v_f \simeq 0.3 C_s$, $D_\perp \simeq 0.1 D_B$ and $E \simeq T_e/L$ where C_s is ion sound velocity, D_B the Bohm diffusion coefficient.

1.2 Model Calculations[1, 7, 8]

In order to understand impurity transport, computer simulations based on the physical model obtained above were perfomed. In the background scrape-off plasma, characterized by T_e, T_i, n_e, v_f and E, a number of test particles (impurities) are traced under the following processes by the Monte-Carlo method: (1)free motion of sputtered impurity atoms, (2)ionization in the background plasma, (3)Coulomb scattering, (4)charge exchange, and (5)perpendicular diffusion of ions.

The results of the simulation with the observed boundary plasma parameters give reasonable values on average ionic charge and the mean energy of the carbon ions in the burial chamber, as shown in Fig.2. Moreover, the temporal impurity behaviour of each charge state through CII to CV is shown to be well simulated by this calculation, as shown in the figure.

From these results the calculation can be applied to a large device. The boundary plasma condition was investigated for JT-60. For the main plasma the parameters are given. Ion sputtering on the limiter/divertor-neutralizer-plate is added to the aforementioned Monte-Carlo calculation.

The formulae for the sputtering yields were given by Sigmunt[9]. These values are, however, several times higher than the experimental data for other heavy ions[10,11]; we have, therefore, divided Sigmund's sputtering yield by two for this calculation, S_0. The energy and the angular distributions of sputtered impurity atoms have been obtained experimentally[12, 13]. We formalize those distributions as[8]:

$$S(E) = \frac{S_o}{(U_o/\beta)^{\beta+1}} E^\beta \exp(-\beta E/U_o) \frac{1}{\Gamma(\beta+1)} \tag{10}$$

$$S(\theta, \varphi) = \frac{S_o}{\pi} \cos\theta \tag{11}$$

where U_0 is the surface binding energy, sublimation energy, β is the fitting constant, $\Gamma(n)$ is the Gamma function and θ is the angle from the normal direction of the sputtered material's surface. Integrals of eqs. (10) and (11)

over E and θ are normalized to S_0, respectively[8]. For simplicity, β is taken to be unity.

Assumed typical parameters are as follows, $\bar{\tau}_p=\bar{\tau}_E=0.7$s, $T_{e0}=T_{i0}=7$keV, $n_{e0}=n_{i0}=7\times10^{13}/cm^3$ and $B_T=4$T. The limiter/neutralizer plates are assumed to be made of molybdenum. Sputtered molybdenum is the only assumed impurity source.

The results are as follows. The average ionic charge of the molybdenum ions $\langle Z_I\rangle$ near the material surface is around 5 in the case with the divertor, and becomes up to 10 without the divertor. These tend to saturate because the sputtered molybdenum ions are forced to return in a shorter time as the temperatures increase (Fig.3(a)).The average energy of the impinging molybdenum ions, $\langle E_I\rangle$, is reduced by a factor of 2 by employing the divertor corresponding to the decrease of ionic charge, as $\langle E_I\rangle=\alpha\langle Z_I\rangle T_b+T_I$, where T_I is the temperature of the molybdenum ions (Fig.3(b)). The stagnation on $\langle E_I\rangle$ is due to the effect of secondary electron emission. If we neglect this effect, the result becomes much different. Impurity growth rates are shown in Fig.3(c). The growth rate is defined by a ratio $N_I(t+\Delta t)/N_I(t)$, where Δt is the impurity recycling characteristic time. Molybdenum impurities continue to increase when the boundary temperature is above 160 eV without the divertor. Owing to radiation cooling, the boundary temperature is in equilibrium at 80-160eV.

In the case without the divertor, we must lose a large portion of the input power, e.g. 80-90%, by radiation and charge-exchange losses (Fig.3(d)). In opposition to this, the molybdenum impurities continue to decrease if the divertor is employed and thus the boundary temperature is not determined by ion sputtering. The boundary temperature increases up to a few hundred eV when radiation and charge-exchange losses are greatly reduced.

1.3 Dense and Cold Divertor Plasma[14]

Dense and cold divertor plasmas with electron density and temperatures of $n_e \gtrsim 5\times10^{13}cm^{-3}$ and $T_e \lesssim 7$eV have been observed previously in Joule-heated Doublet III discharges[15]. Such a dense and cold divertor plasma provides the following advantages:

(a)Because of strong density buildup, the divertor plasma can radiate considerably high power, which leads to a reduction of the heat load onto the divertor plate without deleterious effects to the main plasma.

(b)This sort of divertor is capable of effective particle exhaust, i.e. the exhaust of unused fuel particles, helium ash and other impurities.

(c)Because of a sufficiently low temperature, the erosion of the divertor plates caused by ion sputtering becomes negligibly small.

In this divertor experiment, deuterium plasma is heated for 200ms with a neutral beam injection power of $P_{NB}\simeq1.2$MW. The toroidal field is $B_T=2$T and the plasma current is $I_p=290$kA. The range of the line-averaged electron density of the main plasma is $\bar{n}_e=(1.0\text{-}3.4)\times10^{13}cm^{-3}$ and the central electron temperature is $T_e(0)=1.2\text{-}0.7$keV, at 100ms after the start of beam injection (t=700ms) when most of the measurements were taken.

The separatrix surface intersects the inconel divertor plate on the inner wall of the vacuum vessel. An array of 21 Langmuir probes and 28 thermocouples are installed in the divertor plate in order to measure the vertical profiles of the plasma parameters.

The electron density n_{ed} and temperature T_{ed} at the peak of the density profile on the lower divertor channel are shown in Fig.4 as strong functions of $\bar{n}_e$ or gas puffing($n_{ed}\propto\bar{n}_e^3$). The electron density n_{ed} increases non-linearly from $6\times10^{12}cm^{-3}$ to $2.8\times10^{14}cm^{-3}$, with $\bar{n}_e$ increasing only by a factor of 3.4. At the same time, T_{ed} has cooled down from 30 eV to 3.5eV. The two points profile measurements by the Langmuir probes near the divertor plate show that the temperature gradient along the magnetic field line is found to be very steep ($T_e=36$eV in front of divertor plate and $T_e=8$eV at the divertor plate). The connection length between these two points is 380cm(poloidal

projection length ≃ 16cm). This result (shown with error bars) is well simulated by self consistent fluid model[16] as shown in Fig.5. The total particle flux across the first point of the profile measurement, which is deduced from the ion saturation-current profile, is $\Gamma_p^m \simeq (3.5\text{-}7)\times10^{21}$ particles/s (the flow velocity is assumed to be $v_f=(0.3\text{-}0.6)C_s$). The total particle flux onto the divertor plate is $\Gamma_p^d \simeq 1.6\times10^{22}$ particles/s at $\bar{n}_e=3\times10^{13}cm^{-3}$.

If the divertor plasma in a fusion reactor can be made dense and cold, analogous to the divertor plasma investigated here, the erosion of the divertor plate due to ion sputtering would be negligibly small because of sufficiently low T_{ed} and thus low sheath potential. The threshold energy for ion sputtering is approximately several tens of electron volts for materials such as titanium, iron, nickel, carbon[10].

2. IMPROVEMENT OF ENERGY CONFINEMENT CHARACTERISTICS BY IMPURITY CONTROL[17]

Low-Z materials are attractive for the first wall in a reactor because of the following reasons.

(a) Radiation loss from low-Z impurities is rather small in a high temperature plasma.

(b) The thermal properties of some low-Z material, e.g. carbon, are as good as those of copper or molybdenum.

(c) The self-sputtering yield, which is most closely related to the impurity origin, is smaller than that of the high-Z materials such as Mo. Therefore, the wall erosion is rather low.

Here we show an example of improvement of energy confinement time with controlling impurity by means of applying carbon wall.

Figure 6 shows the profiles of electron temperature and density for (a) carbon wall and (b) Ti-flushed wall. For carbon wall case, P_R+P_{CX} that dominated by carbon line radiation is shown to be increased and concentrated more in plasma periphery compared with Ti wall case. Consequently, the boundary electron temperature is cooled down due to increase of P_R+P_{CX} obeying eq.(6). As the result, the effective radius of plasma pressure profile increases and thus the energy confinement time is improved by a factor of 2 by employing carbon wall with divertor as shown in Fig.7. The effect of the impulity control by a divertor on improvement of energy confinement time is also shown in the figure.

Chemical sputtering is shown to be easily suppressed by prebombardment of hydrogen ions at the substratum temperature above 500°C.

3. IMPROVEMENT OF ENERGY CONFINEMENT CHARACTERISTICS BY FUEL PARTICLE CONTROL

The good confinement discharge with divertor beam-heated plasma, so called H-mode, can be criated by optimaized gas fueling in Doublet III[18] as shown in Fig.8. Increasing edge recycling (H_αLIM) leads to degradation of confinement characteristics. This implys that the control of fuel particle is responsible to the improvement of confinement properties.

Pellet injection is shown to be effective to reduce edge fueling and be able to improve confinement characteristics especially in high density region in both Joule- and beam-heated discharges[19,20].

In gas-fueled divertor ohmic discharges, the recycling and the neutral pressure both at the edge and the divertor region, increase nonlinearly as the density is raised above $4\times10^{13}cm^{-3}$. The energy confinement time saturates around 60ms (Fig.9). In contrast to that, the pellet fueled confinement time continue to improve with increased density. This is probably due to the fact that in the pellet fueled discharges both the edge pressure and the limiter recycling light are maintained at relatively low levels (Fig.9) and/or the successful density rise at the plasma center which has good

projection length ≈ 16cm). This result (shown with error bars) is well simulated by self consistent fluid model[16] as shown in Fig.5. The total particle flux across the first point of the profile measurement, which is deduced from the ion saturation-current profile, is $\Gamma_p^m \simeq (3.5\text{-}7)\times10^{21}$ particles/s (the flow velocity is assumed to be $v_f=(0.3\text{-}0.6)C_s$). The total particle flux onto the divertor plate is $\Gamma_p^d \simeq 1.6\times10^{22}$ particles/s at $\bar{n}_e=3\times10^{13}cm^{-3}$.

If the divertor plasma in a fusion reactor can be made dense and cold, analogous to the divertor plasma investigated here, the erosion of the divertor plate due to ion sputtering would be negligibly small because of sufficiently low T_{ed} and thus low sheath potential. The threshold energy for ion sputtering is approximately several tens of electron volts for materials such as titanium, iron, nickel, carbon[10].

2. IMPROVEMENT OF ENERGY CONFINEMENT CHARACTERISTICS BY IMPURITY CONTROL[17]

Low-Z materials are attractive for the first wall in a reactor because of the following reasons.

(a)Radiation loss from low-Z impurities is rather small in a high temperature plasma.

(b)The thermal properties of some low-Z material, e.g. carbon, are as good as those of copper or molybdenum.

(c)The self-sputtering yield, which is most closely related to the impurity origin, is smaller than that of the high-Z materials such as Mo. Therefore, the wall erosion is rather low.

Here we show an example of improvement of energy confinement time with controlling impurity by means of applying carbon wall.

Figure 6 shows the profiles of electron temperature and density for (a) carbon wall and (b)Ti-flushed wall. For carbon wall case, P_R+P_{CX} that dominated by carbon line radiation is shown to be increased and concentrated more in plasma periphery compared with Ti wall case. Consequently, the boundary electron temperature is cooled down due to increase of P_R+P_{CX} obeying eq.(6). As the result, the effective radius of plasma pressure profile increases and thus the energy confinement time is improved by a factor of 2 by employing carbon wall with divertor as shown in Fig.7. The effect of the impulity control by a divertor on improvement of energy confinement time is also shown in the figure.

Chemical sputtering is shown to be easily suppressed by prebombardment of hydrogen ions at the substratum temperature above 500°C.

3. IMPROVEMENT OF ENERGY CONFINEMENT CHARACTERISTICS BY FUEL PARTICLE CONTROL

The good confinement discharge with divertor beam-heated plasma, so called H-mode, can be criated by optimaized gas fueling in Doublet III[18] as shown in Fig.8. Increasing edge recycling (H_αLIM) leads to degradation of confinement characteristics. This implys that the control of fuel particle is responsible to the improvement of confinement properties.

Pellet injection is shown to be effective to reduce edge fueling and be able to improve confinement characteristics especially in high density region in both Joule- and beam-heated discharges[19,20].

In gas-fueled divertor ohmic discharges, the recycling and the neutral pressure both at the edge and the divertor region, increase nonlinearly as the density is raised above $4\times10^{13}cm^{-3}$. The energy confinement time saturates around 60ms (Fig.9). In contrast to that, the pellet fueled confinement time continue to improve with increased density. This is probably due to the fact that in the pellet fueled discharges both the edge pressure and the limiter recycling light are maintained at relatively low levels (Fig.9) and/or the successful density rise at the plasma center which has good

projection length ≈ 16cm). This result (shown with error bars) is well simulated by self consistent fluid model[16] as shown in Fig.5. The total particle flux across the first point of the profile measurement, which is deduced from the ion saturation-current profile, is $\Gamma_p^m \simeq (3.5\text{-}7)\times10^{21}$ particles/s (the flow velocity is assumed to be $v_f=(0.3\text{-}0.6)C_s$). The total particle flux onto the divertor plate is $\Gamma_p^d \simeq 1.6\times10^{22}$ particles/s at $\bar{n}_e=3\times10^{13}cm^{-3}$.

If the divertor plasma in a fusion reactor can be made dense and cold, analogous to the divertor plasma investigated here, the erosion of the divertor plate due to ion sputtering would be negligibly small because of sufficiently low T_{ed} and thus low sheath potential. The threshold energy for ion sputtering is approximately several tens of electron volts for materials such as titanium, iron, nickel, carbon[10].

2. IMPROVEMENT OF ENERGY CONFINEMENT CHARACTERISTICS BY IMPURITY CONTROL[17]

Low-Z materials are attractive for the first wall in a reactor because of the following reasons.

(a)Radiation loss from low-Z impurities is rather small in a high temperature plasma.

(b)The thermal properties of some low-Z material, e.g. carbon, are as good as those of copper or molybdenum.

(c)The self-sputtering yield, which is most closely related to the impurity origin, is smaller than that of the high-Z materials such as Mo. Therefore, the wall erosion is rather low.

Here we show an example of improvement of energy confinement time with controlling impurity by means of applying carbon wall.

Figure 6 shows the profiles of electron temperature and density for (a) carbon wall and (b)Ti-flushed wall. For carbon wall case, P_R+P_{CX} that dominated by carbon line radiation is shown to be increased and concentrated more in plasma periphery compared with Ti wall case. Consequently, the boundary electron temperature is cooled down due to increase of P_R+P_{CX} obeying eq.(6). As the result, the effective radius of plasma pressure profile increases and thus the energy confinement time is improved by a factor of 2 by employing carbon wall with divertor as shown in Fig.7. The effect of the impulity control by a divertor on improvement of energy confinement time is also shown in the figure.

Chemical sputtering is shown to be easily suppressed by prebombardment of hydrogen ions at the substratum temperature above 500°C.

3. IMPROVEMENT OF ENERGY CONFINEMENT CHARACTERISTICS BY FUEL PARTICLE CONTROL

The good confinement discharge with divertor beam-heated plasma, so called H-mode, can be criated by optimaized gas fueling in Doublet III[18] as shown in Fig.8. Increasing edge recycling (H_αLIM) leads to degradation of confinement characteristics. This implys that the control of fuel particle is responsible to the improvement of confinement properties.

Pellet injection is shown to be effective to reduce edge fueling and be able to improve confinement characteristics especially in high density region in both Joule- and beam-heated discharges[19,20].

In gas-fueled divertor ohmic discharges, the recycling and the neutral pressure both at the edge and the divertor region, increase nonlinearly as the density is raised above $4\times10^{13}cm^{-3}$. The energy confinement time saturates around 60ms (Fig.9). In contrast to that, the pellet fueled confinement time continue to improve with increased density. This is probably due to the fact that in the pellet fueled discharges both the edge pressure and the limiter recycling light are maintained at relatively low levels (Fig.9) and/or the successful density rise at the plasma center which has good

confinement properties. Preliminal analysis with 1-D tokamak code shows good agreement with experimental results, i.e. low edge recycling, peaked density profile and proportional increase of τ_E with $\bar{n}_e$, with assuming no change in ion transport characteristics before and after pellet injection[21] which is in contrast to the result from ALCATOR-C[22].

During continuous neutral beam heating of very high density plasmas, the confinement times remain near the improved ohmic level for the first ≈60ms but then rapidly deteriorate corresponding to the increase of edge ablation. Figure 10 shows the successful central electron density rise due to pellet fueling during Joule-heating phase of a limiter discharge. But in the NB-heating phase, the edge density and the edge recycling start to increase when the fast ions from neutral beam build up.

A scheme was tested to enhance pellet penetration and reduce pellet ablation at plasma edge by briefly interrupting the neutral beams just before each pellet was injected. This is based on the relatively fast slowing-down time of fast ions in the edge plasma which is less than 10ms, and the expected dependence of the ablation on the fast ion population[23]. The energy confinement time and pellet penetration are improved over the continuous beam case for delay times not less than 8ms. Furter delay shows little additional improvement (Fig.11).

A comparison of pellet ablation profiles for continuous vs. interrupted beam (Fig.12) shows that there is no significant difference in pellet penetration. However, the pellet ablation in the outer 10cm of the plasma is reduced by interrupting the beam. The reduction in the edge density and slower central density decay time as measured by the visible bremsstrahlung array. This reduction of edge ablation may account for the maintained improvement of the energy confinement time keeping low edge recycling (Fig.11-b)).

The combination of the improved confinement and the high densities has produced a significant extention of the $\bar{n}_e$, τ_E^* diagram (Fig.13) for Doublet III. The Lawson product $n_e(0)\cdot\tau_E^*$ is increased by a factor of 3 to 4 in both limiter and divertor discharges. The neutron production rate has been improved by a factor of 10 over limiter beam-heated plasmas of comparable gas fueled discharges. These results are very encouraging for large nondivertor tokamaks that will rely heavily on neutral beam heating to produce energy breakeven conditions.

4. DISCUSSION AND CONCLUSION

Physical models of divertor/boundary plasmas and the divertor functions about impurity control are empilically obtained. It is shown that the active controls of both impurity and fuel particles are highly responsible to improve the plasma confinement characteristics.

The control flow-chart of plasma-surface interactions is presented in Fig.14. It is demonstrated that the control (decreasing) of plasma-surface interaction can improve energy confinement time.

For more precise modeling or understanding of such a system, following atomic data base are required:

(1)Cross sections or rate coefficients of following various processes in the back ground plasmas for the parameter ranges T_e=4-200eV and $n_e=10^{12}$-10^{14}cm^{-3}:

- °ionization
- °charge exchange
- °radiative cooling rate (especially at several tens eV)
- °recycling rate for various materials
- °dissociation

(2)Pellet ablation model with high energy ions

The methods of controlling of the recycling rate (e.g. control the wall temperature etc.) and of optimized impurity radiative cooling should also be investigated.

confinement properties. Preliminal analysis with 1-D tokamak code shows good agreement with experimental results, i.e. low edge recycling, peaked density profile and proportional increase of τ_E with $\bar{n}_e$, with assuming no change in ion transport characteristics before and after pellet injection[21] which is in contrast to the result from ALCATOR-C[22].

During continuous neutral beam heating of very high density plasmas, the confinement times remain near the improved ohmic level for the first ≈60ms but then rapidly deteriorate corresponding to the increase of edge ablation. Figure 10 shows the successful central electron density rise due to pellet fueling during Joule-heating phase of a limiter discharge. But in the NB-heating phase, the edge density and the edge recycling start to increase when the fast ions from neutral beam build up.

A scheme was tested to enhance pellet penetration and reduce pellet ablation at plasma edge by briefly interrupting the neutral beams just before each pellet was injected. This is based on the relatively fast slowing-down time of fast ions in the edge plasma which is less than 10ms, and the expected dependence of the ablation on the fast ion population[23]. The energy confinement time and pellet penetration are improved over the continuous beam case for delay times not less than 8ms. Furter delay shows little additional improvement (Fig.11).

A comparison of pellet ablation profiles for continuous vs. interrupted beam (Fig.12) shows that there is no significant difference in pellet penetration. However, the pellet ablation in the outer 10cm of the plasma is reduced by interrupting the beam. The reduction in the edge density and slower central density decay time as measured by the visible bremsstrahlung array. This reduction of edge ablation may account for the maintained improvement of the energy confinement time keeping low edge recycling (Fig.11-b)).

The combination of the improved confinement and the high densities has produced a significant extention of the $\bar{n}_e$, τ_E^* diagram (Fig.13) for Doublet III. The Lawson product $n_e(0)\cdot\tau_E^*$ is increased by a factor of 3 to 4 in both limiter and divertor discharges. The neutron production rate has been improved by a factor of 10 over limiter beam-heated plasmas of comparable gas fueled discharges. These results are very encouraging for large nondivertor tokamaks that will rely heavily on neutral beam heating to produce energy breakeven conditions.

4. DISCUSSION AND CONCLUSION

Physical models of divertor/boundary plasmas and the divertor functions about impurity control are empilically obtained. It is shown that the active controls of both impurity and fuel particles are highly responsible to improve the plasma confinement characteristics.

The control flow-chart of plasma-surface interactions is presented in Fig.14. It is demonstrated that the control (decreasing) of plasma-surface interaction can improve energy confinement time.

For more precise modeling or understanding of such a system, following atomic data base are required:

(1)Cross sections or rate coefficients of following various processes in the back ground plasmas for the parameter ranges T_e=4-200eV and $n_e=10^{12}$-10^{14}cm^{-3}:

- °ionization
- °charge exchange
- °radiative cooling rate (especially at several tens eV)
- °recycling rate for various materials
- °dissociation

(2)Pellet ablation model with high energy ions

The methods of controlling of the recycling rate (e.g. control the wall temperature etc.) and of optimized impurity radiative cooling should also be investigated.

Acknowledgement

The author is grateful to both DIVA and Doublet III operations and physics groups for their great helps and fruitful discussions. He also acknowledges the continuing encouragements of Drs. M. Tanaka, M. Yoshikawa, K. Tomabechi and S. Mori.

References

[1]S. SENGOKU and H. OHTSUKA, J. Nucl. Mat. 93/94(1980)75.
[2]Y. SHIMOMURA et al., Japan Atomic Energy Research Inst. Rep., JAERI-M 7457 (1979).
[3]DIVA Group, Nucl. Fusion 18(1978)1619.
[4]H. KIMURA et al., Nucl. Fusion 18(1978)1195.
[5]Y. SHIMOMURA and H. MAEDA, J. Nucl. Mat. 76/77(1978)45.
[6]G.D. HOBBS and J.A. WESSON, Culham Lab. Rep. CLM-R61(1966).
[7]S. SENGOKU et al., Japan Atomic Energy Research Inst. Rep. JAERI-M 7918 (1978).
[8]S. SENGOKU et al., Nucl. Fusion 19(1979)1327.
[9]P. SIGMUND, Phys. Rev. 184(1969)383.
[10]B.M.U. SCHERZER et al., in Plasma Wall Interaction(Proc. Int. Symp. Jülich, 1976) Pergamon Press, Oxford (1977)353.
[11]C.F. BARNET et al., Oak Ridge Nat. Lab. Rep. ORNL -5207(1977)D.1.30.
[12]P. HUCKS et al., J. Nucl. Mat. 76/77(1978)136.
R.V. STUART et al., J. App. Phys. 40(1969)803.
[13]M. KAMINSKY, "Atomic and Ionic Impact Phenomena on Metal Surface", Springer Verlag(1965)Berlin, p.169.
[14]S. SENGOKU et al., Nucl. Fusion 24(1984)415.
[15]M. SHIMADA et al., Nucl. Fusion 22(1982)643.
[16]S. SAITO et al., J. Nucl. Mat. 128/129(1984)131.
[17]S. SENGOKU et al., J. Nucl. Mat.93/94(1980)178.
[18]M. NAGAMI et al., Nucl. Fusion 24(1984)183.
[19]S. SENGOKU et al., in Plasma Phys. Controlled Nucl. Fusion Res. (Proc. 10th Int. Conf., London, 1984)Vol.1, IAEA, Vienna (1985)405.
[20]S. SENGOKU et al.,"Improvement of Energy Confinement Time by Continuous Pellet Fueling in Beam Heated Doublet III Limiter Discharges", Nucl. Fusion 25(1985)1475.
[21]S. SENGOKU, Japan Atomic Energy Research Inst. Rep. JAERI-M 85-102 (1985).
[22]M. GREENWALD et al., in Plasma Phys. and Controlled Nucl. Fusion Res. (Pro. 10th Int. Conf., London, 1984) IAEA,Vienna, paper IAEA-CN-44/A-I-3.
[23]S.L. MILORA, Oak Ridge National Lab. Rep. ORNL/TM-8616 (1983).

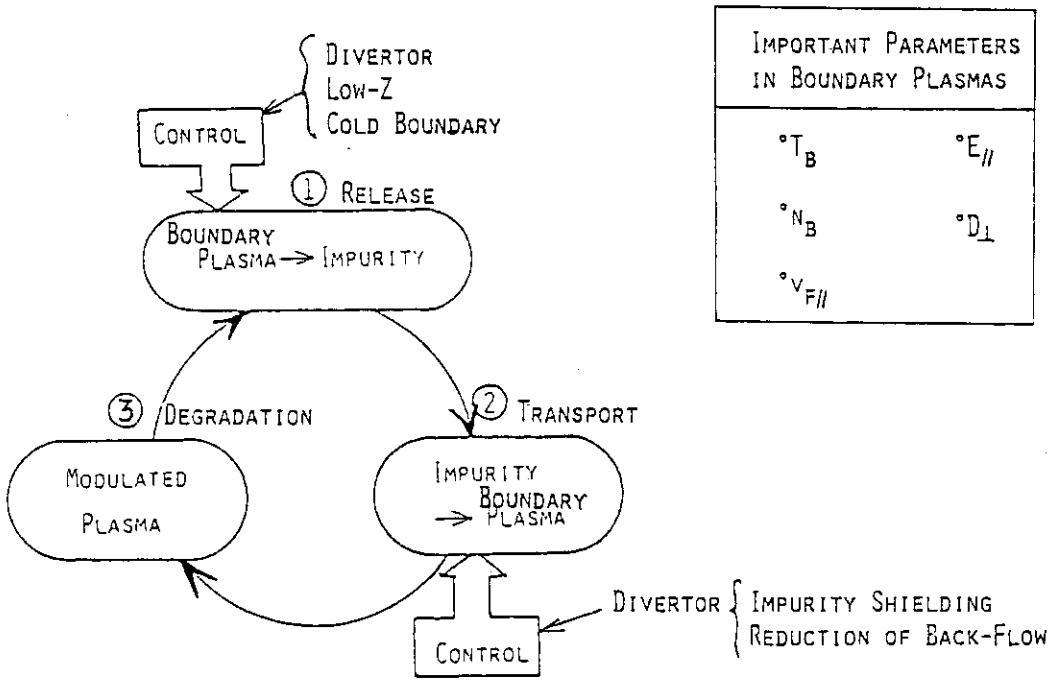

Fig. 1 Cyclic process of plasma–surface interaction.

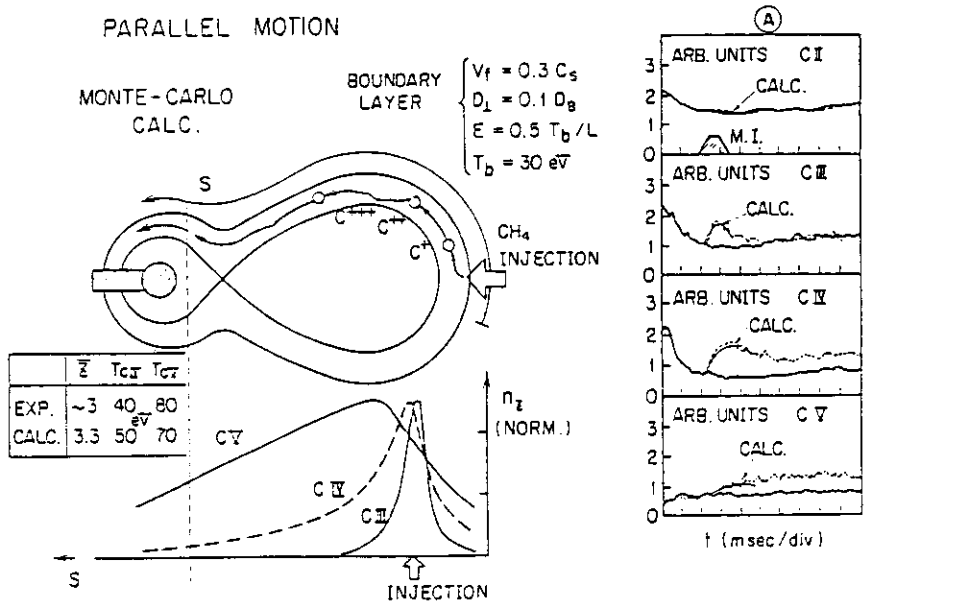

Fig. 2 Result of Monte-Carlo calculation of CH_4 injection experiment. Temporal behaviour Ⓐ, average charge state, $\bar{z}$, and average energies of carbon ions, T_{CIV} and T_{CV}, are shown. These are in good agreement with the experiment.

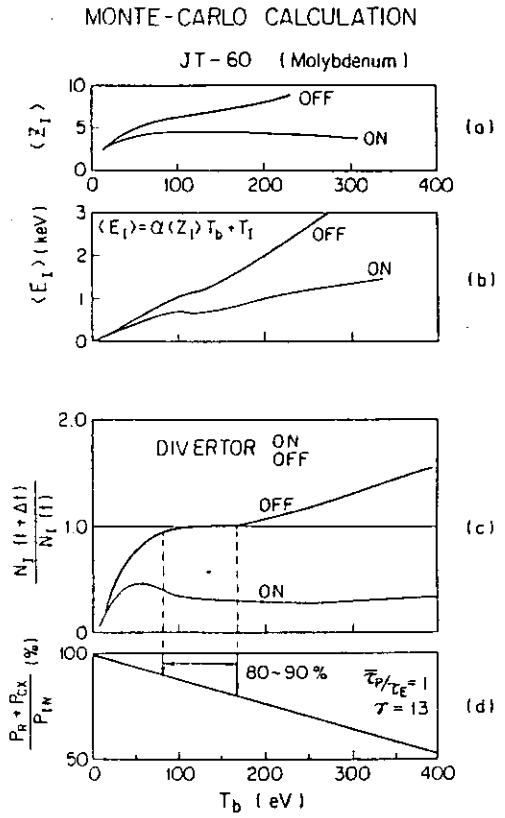

Fig. 3 Results of the simulation for molybdenum impurity recycling in JT-60: (a) average charge states, $\langle Z_I \rangle$; (b) average sputtering energies, $\langle E_I \rangle$; (c) impurity growth rate, $N_I(t+\Delta t)/N_I(t)$; and (d) the ratio of radiation and charge-exchange power losses to input power, as functions of the electron temperature in the boundary plasma, T_b

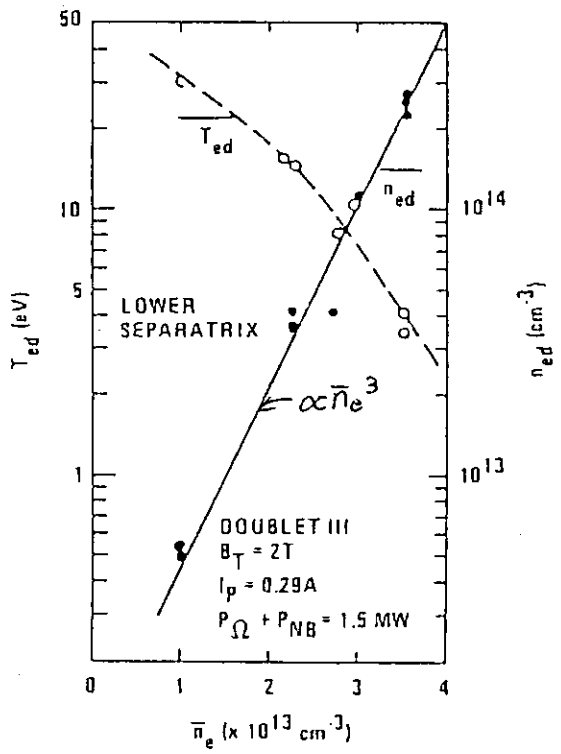

Fig. 4 Electron density, n_{ed} (—●—), and temperature, T_{ed} (--○--), at the peaks of the density profile on the divertor plate as a function of the average electron density of the main plasma $\bar{n}_e$ (t = 700 ms).

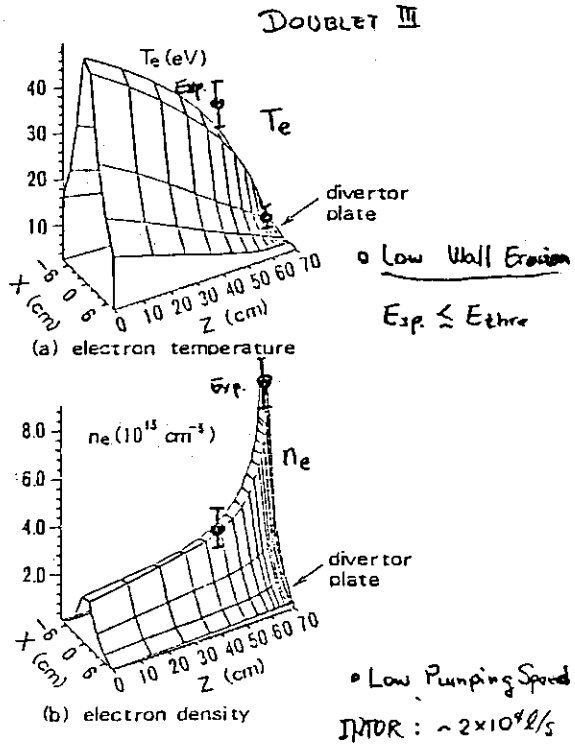

Fig. 5 Two dimensional distributions of the divertor plasma. (a) Electron temperature. (b) Electron density.

$f_{He} < 5\%$

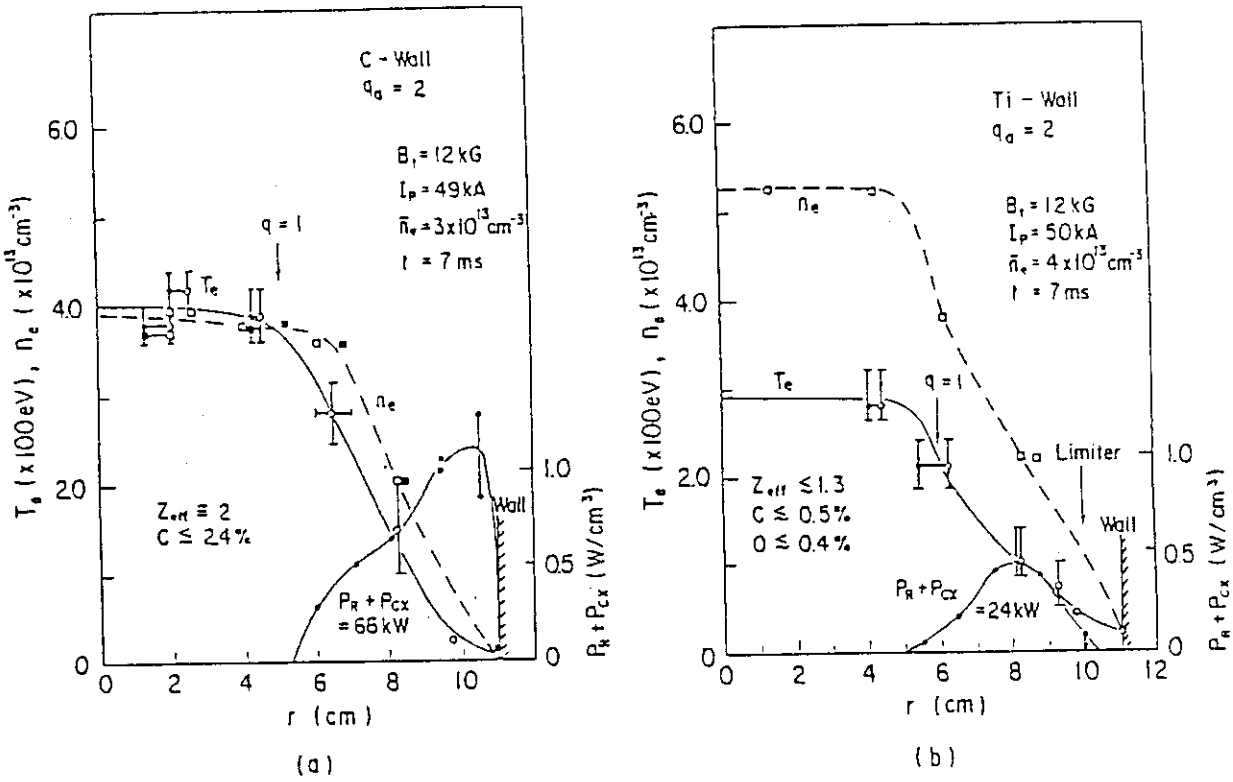

Fig. 6 Spatial distributions of electron temperature (T_e), density (n_e) and radiation and charge exchange loss power (P_R+P_{CX}) for (a) carbon and (b) titanium walls.

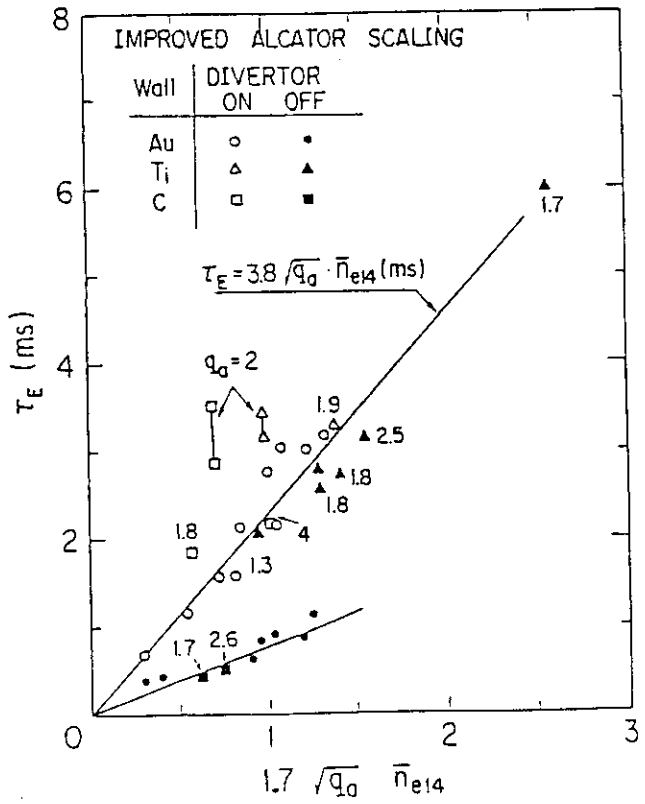

Fig. 7 τ_E vs. $1.7\sqrt{q}\bar{n}_{e14}$, where $\bar{n}_{e14}$ is the line-averaged density in 10^{14} cm^{-3} and τ_E is in ms. Au wall (○, ●), Ti wall (△, ▲) and C wall (□, ■) are investigated with divertor (○, △, □) and without divertor (●, ▲, ■).

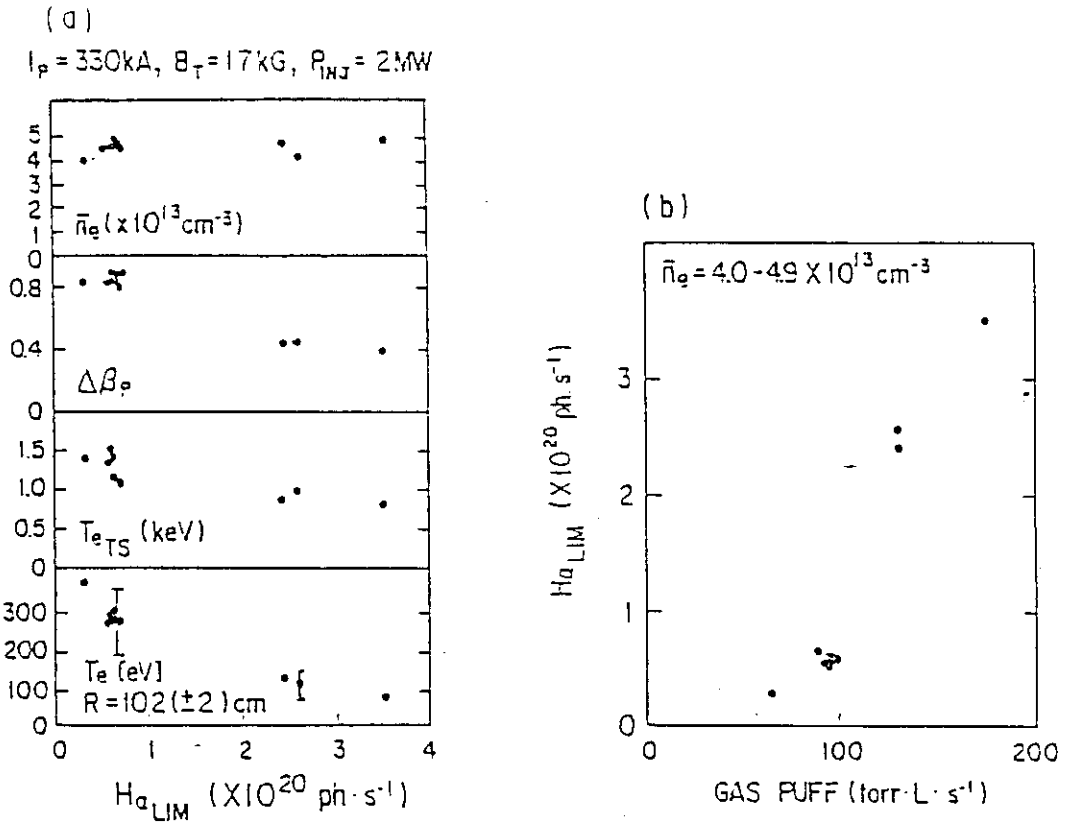

Fig. 8 (a) $\Delta\beta_p$, T_{eTS}, and electron temperature near the main separatrix magnetic surface versus $H_{\alpha LIM}$ for discharges with similar $\bar{n}_e$ [(4-4.9)×10^{13} cm^{-3}]. Only the intensity of the cold-gas puff was changed during the beam injection for these discharges; (b) $H_{\alpha LIM}$ versus gas puff intensity.

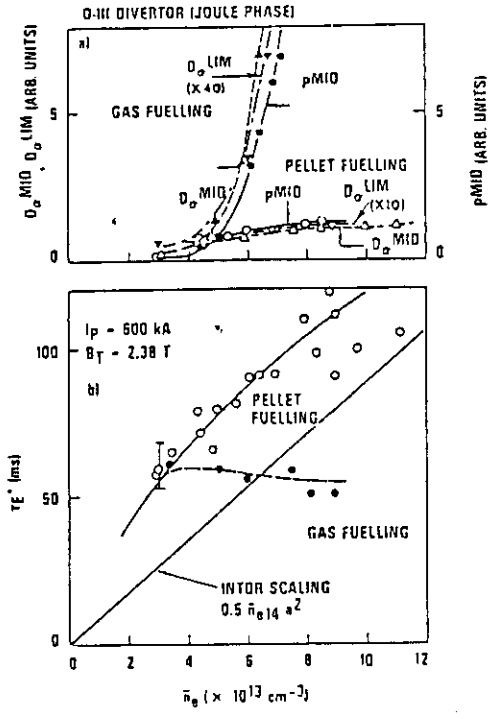

Fig. 9 *Comparison of a) particle recycling at limiter and divertor regions as inferred from D_α^{LIM} and D_α^{MID} and neutral pressure at divertor region and b) the energy confinement time between gas- and pellet-fuelled discharges as functions of $\bar{n}_e$. Open symbols denote pellet-fuelled, and solid symbols gas-fuelled discharges.*

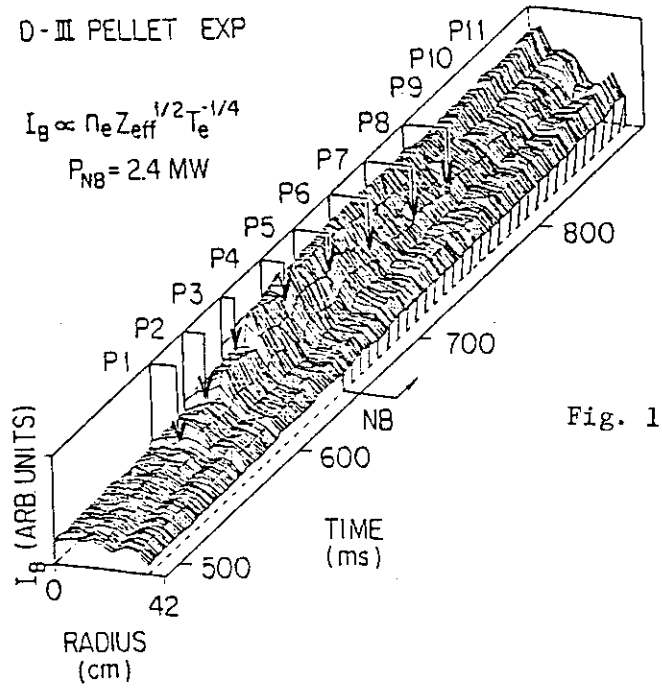

Fig. 10 Temporal and spatial evolution of Abel inverted square root of Bremsstrahlung emission as a relative density profile evolution ($I_\beta \propto n_e Z_{eff}^{1/2} T_e^{-1/4}$) for the pellet fueled discharge. Signals are filtered by 500 Hz low-pass filter and sliced in every 1 ms. The pellet penetration for pellet numbers 1-8 (P1-P8) are shown by arrows. The neutral beam injection period is shown by the hatched area.

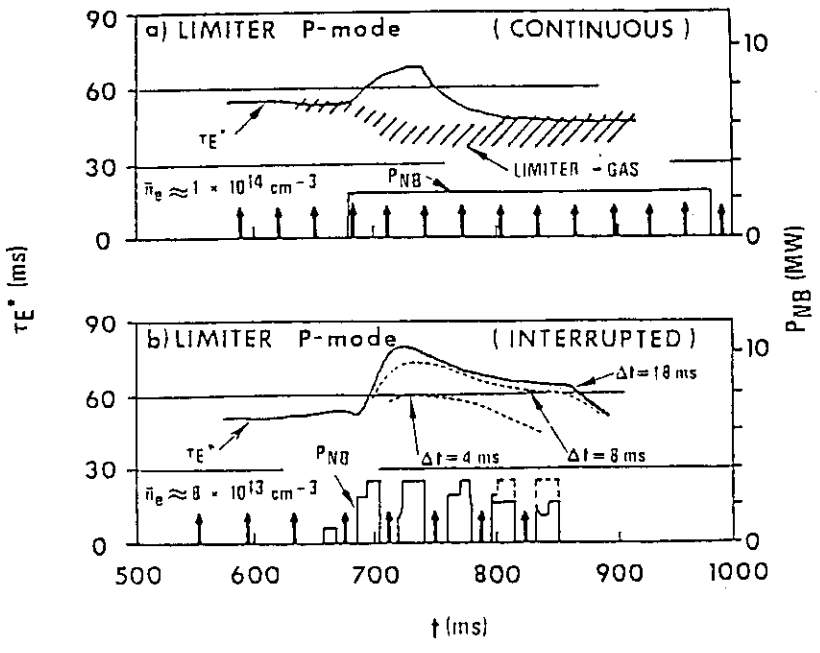

Fig. 11 Comparison of temporal deviation of average energy confinement time for a) continuous beam case and b) interrupted beam case for Δt=4, 8 and 18 ms
Pellet injection timings are shown by arrows except for Δt=4 and 18 ms.

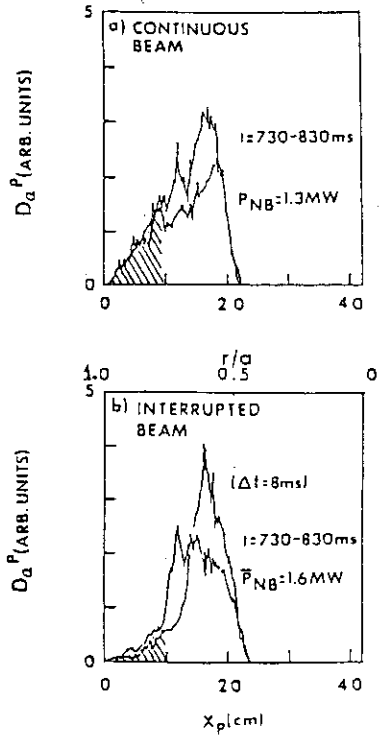

Fig. 12 D_α signals coming from pellets to 90° filtered photodiode ($D_\alpha{}^P$) as the pellet ablation profiles: a) for continuous 1.3 MW beam heating and b) for interrupted beam heating (averaged beam power of 1.6 MW), in Fig. 11 (Δt=8 ms). Penetration is measured from the limiter surface, X_p, deduced from measured pellet velocity (800 m/s). Those pellets are injected between t=730 ms and 830 ms in both cases.

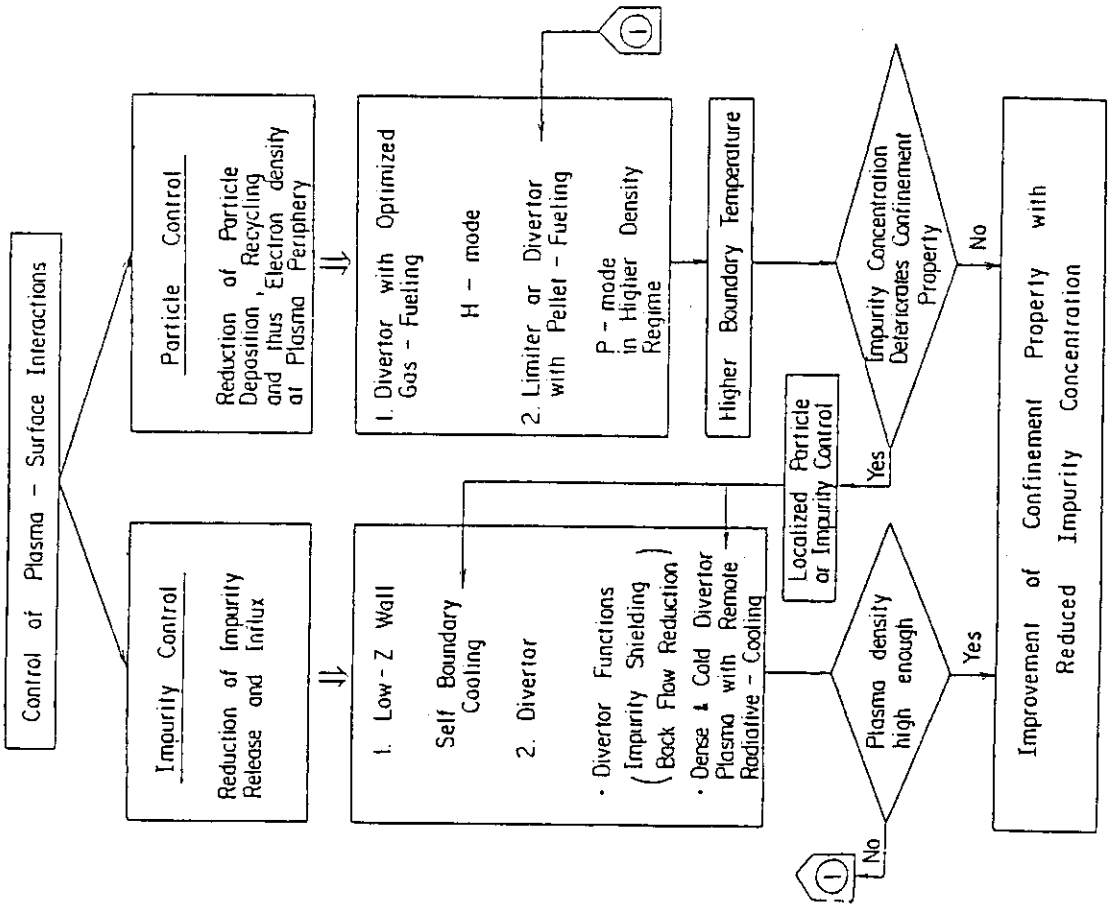

Fig. 14 Control flow-chart of plasma-surface interaction.

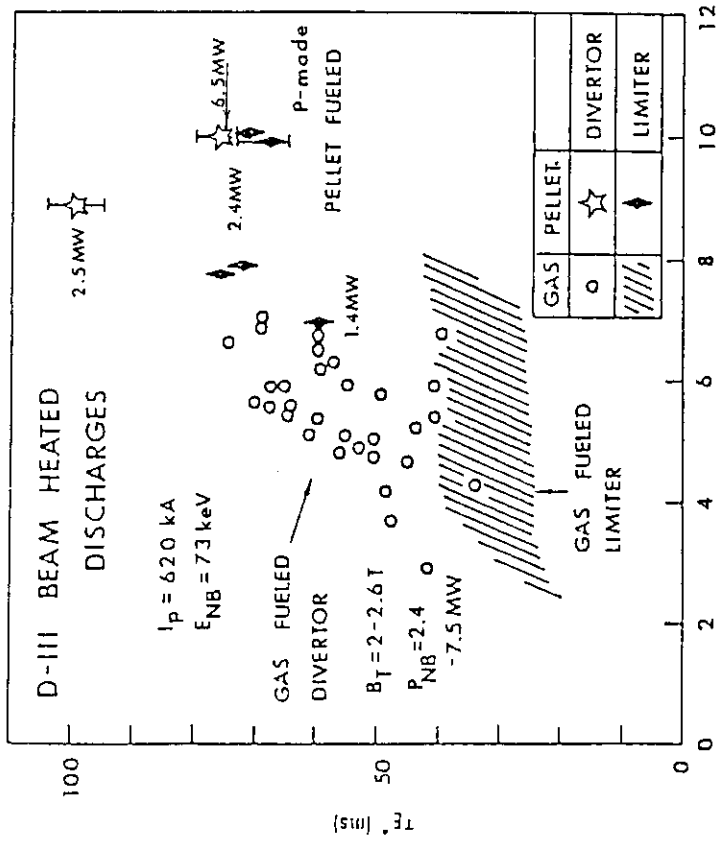

Fig. 13 Comparison of $\bar{n}_e$, τ_E^* plot between pellet and gas fueled discharges for both limiter and divertor configurations with continuous beams. The upper envelope of open circles corresponds to D-III H-mode discharges. For gas fueled discharges, τ_E^* is calculated when dW/dt = 0.